



ARL-TR-7255 • MAR 2015



# **Sparse Matrix Motivated Reconstruction of Far-Field Radiation Patterns**

**by Berenice Verdin and Patrick Debroux**

Approved for public release; distribution unlimited.

## **NOTICES**

### **Disclaimers**

The findings in this report are not to be construed as an official Department of the Army position unless so designated by other authorized documents.

Citation of manufacturer's or trade names does not constitute an official endorsement or approval of the use thereof.

Destroy this report when it is no longer needed. Do not return it to the originator.



# **Sparse Matrix Motivated Reconstruction of Far-Field Radiation Patterns**

**by Berenice Verdin and Patrick Debroux**  
*Survivability/Lethality Analysis Directorate, ARL*

| REPORT DOCUMENTATION PAGE  |                             |                              |                                      | Form Approved<br>OMB No. 0704-0188                          |   |
|--|-----------------------------|------------------------------|--------------------------------------|---|---|
| <p>Public reporting burden for this collection of information is estimated to average 1 hour per response, including the time for reviewing instructions, searching existing data sources, gathering and maintaining the data needed, and completing and reviewing the collection information. Send comments regarding this burden estimate or any other aspect of this collection of information, including suggestions for reducing the burden, to Department of Defense, Washington Headquarters Services, Directorate for Information Operations and Reports (0704-0188), 1215 Jefferson Davis Highway, Suite 1204, Arlington, VA 22202-4302. Respondents should be aware that notwithstanding any other provision of law, no person shall be subject to any penalty for failing to comply with a collection of information if it does not display a currently valid OMB control number.</p> <p><b>PLEASE DO NOT RETURN YOUR FORM TO THE ABOVE ADDRESS.</b></p>  |                             |                              |                                      |   |   |
| 1. REPORT DATE (DD-MM-YYYY)<br>Mar 2015  |                             | 2. REPORT TYPE<br>Final      |                                      | 3. DATES COVERED (From - To)<br>08/2015                     |   |
| 4. TITLE AND SUBTITLE<br>Sparse Matrix Motivated Reconstruction of Far-Field Radiation Patterns  |                             |                              |                                      | 5a. CONTRACT NUMBER   |   |
|  |                             |                              |                                      | 5b. GRANT NUMBER  |   |
|  |                             |                              |                                      | 5c. PROGRAM ELEMENT NUMBER                                  |   |
| 6. AUTHOR(S)<br>Berenice Verdin and Patrick Debroux  |                             |                              |                                      | 5d. PROJECT NUMBER  |   |
|  |                             |                              |                                      | 5e. TASK NUMBER   |   |
|  |                             |                              |                                      | 5f. WORK UNIT NUMBER  |   |
| 7. PERFORMING ORGANIZATION NAME(S) AND ADDRESS(ES)<br>US Army Research Laboratory<br>ATTN: RDRL-SLE-E<br>White Sands Missile Range, NM 88002   |                             |                              |                                      | 8. PERFORMING ORGANIZATION REPORT NUMBER<br><br>ARL-TR-7255 |   |
| 9. SPONSORING/MONITORING AGENCY NAME(S) AND ADDRESS(ES)<br>Oak Ridge Associated Universities (ORAU)<br>4692 Millennium Drive Suite 101 Belcamp, MD 21017   |                             |                              |                                      | 10. SPONSOR/MONITOR'S ACRONYM(S)                            |   |
|  |                             |                              |                                      | 11. SPONSOR/MONITOR'S REPORT NUMBER(S)                      |   |
| 12. DISTRIBUTION/AVAILABILITY STATEMENT<br>Approved for public release; distribution unlimited.  |                             |                              |                                      |   |   |
| 13. SUPPLEMENTARY NOTES  |                             |                              |                                      |   |   |
| 14. ABSTRACT<br><p>The measurement of radiation patterns is time consuming and expensive. Therefore, a novel technique that reduces samples required to measure radiation patterns is proposed where random samples are taken to reconstruct 2-dimensional (2-D) or 3-dimensional (3-D) far-field radiation patterns. The proposed technique uses a compressive sensing algorithm based on sparse representations of radiation patterns using the inverse Discrete Fourier Transform (DFT) and the inverse Discrete Cosine Transform (DCT). The algorithm was evaluated by using 3 antennas modeled with the high-frequency structural simulator (HFSS): a half-wave dipole, a Vivaldi, and a pyramidal horn. The 2-D radiation pattern was reconstructed for each antenna using less than 44% of the total number of measurements with low-root mean square error (RMSE). In addition, the proposed reconstruction algorithm was evaluated using measured data obtained in an anechoic chamber. The 3-D radiation patterns of a pyramidal horn antenna was reconstructed by using only 13% of the total number of measurements. By using the proposed approach for radiation pattern reconstruction, the time required to take measurements in an anechoic chamber can be reduced up to 87%, therefore ensuring a good reconstruction with very low-RMSE in the case of a directive antenna such as the pyramidal horn.</p> |                             |                              |                                      |   |   |
| 15. SUBJECT TERMS<br>compressive sensing, far field measurements, radiation patterns   |                             |                              |                                      |   |   |
| 16. SECURITY CLASSIFICATION OF:  |                             |                              | 17. LIMITATION OF ABSTRACT<br><br>UU | 18. NUMBER OF PAGES<br><br>30                               | 19a. NAME OF RESPONSIBLE PERSON<br>Berenice Verdin        |
| a. REPORT<br>Unclassified  | b. ABSTRACT<br>Unclassified | c. THIS PAGE<br>Unclassified |                                      |   | 19b. TELEPHONE NUMBER (Include area code)<br>575-678-5384 |

## Contents

---

|  |           |
|--|-----------|
| <b>List of Figures</b>   | <b>iv</b> |
| <b>1. Introduction</b>   | <b>1</b>  |
| <b>2. Compressive Sensing Theory</b>   | <b>2</b>  |
| Compressive Sensing Applied to Far-Field Radiation Patterns                            | 2         |
| <b>3. Evaluation of the Compressive Sensing Reconstruction Algorithm by Simulation</b> | <b>4</b>  |
| 3.1 Half-Wave Dipole Antenna   | 5         |
| 3.2 Vivaldi Antenna  | 8         |
| 3.3 Pyramidal Horn Antenna   | 11        |
| <b>4. Evaluation of the Compressive Sensing Reconstruction Algorithm by Experiment</b> | <b>13</b> |
| <b>5. Conclusions</b>  | <b>18</b> |
| <b>6. References</b>   | <b>20</b> |
| <b>List of Symbols, Abbreviations, and Acronyms</b>                                    | <b>22</b> |
| <b>Distribution List</b>   | <b>23</b> |

## List of Figures

|         |   |    |
|---------|---|----|
| Fig. 1  | Compressive sensing algorithm for 3-D radiation patterns .....  | 4  |
| Fig. 2  | Random samples taken from the simulated 2-D radiation pattern of a vertical half-wave dipole at $\theta = 90^\circ$ .....               | 5  |
| Fig. 3  | Reconstructed radiation pattern compared to the simulated radiation pattern of a vertical half-wave dipole at $\theta = 90^\circ$ ..... | 6  |
| Fig. 4  | Random measurements taken from the simulated radiation pattern of a horizontal half-wave dipole at $\phi = 0^\circ$ .....               | 6  |
| Fig. 5  | Reconstructed radiation pattern compared to the simulated radiation pattern of a horizontal half-wave dipole at $\phi = 0^\circ$ .....  | 7  |
| Fig. 6  | Mean RMSE of the reconstructed radiation pattern for the horizontal half-wave dipole for $\phi = 0^\circ$ .....                         | 8  |
| Fig. 7  | Simulated radiation pattern and random samples used for reconstruction of the Vivaldi antenna .....                                     | 9  |
| Fig. 8  | Simulated radiation pattern and reconstructed radiation pattern of the Vivaldi antenna .....  | 10 |
| Fig. 9  | RMSE mean of the reconstructed radiation pattern for the Vivaldi antenna .....  | 11 |
| Fig. 10 | Simulated radiation pattern and measurements taken for the horn antenna .....   | 11 |
| Fig. 11 | Simulated radiation pattern and reconstructed radiation pattern for the horn antenna .....  | 12 |
| Fig. 12 | RMSE mean of the reconstructed radiation pattern for the horn antenna .....   | 13 |
| Fig. 13 | 2-D radiation pattern of the pyramidal horn (anechoic chamber) antenna and measurements used for reconstruction .....                   | 14 |
| Fig. 14 | Anechoic chamber radiation pattern and reconstructed radiation pattern for the pyramidal horn antenna .....                             | 15 |
| Fig. 15 | Mean RMSE of the reconstructed empirical radiation pattern for the pyramidal horn antenna .....   | 16 |
| Fig. 16 | The empirical 3-D radiation pattern and samples used for reconstruction for the pyramidal horn antenna .....                            | 16 |
| Fig. 17 | Reconstructed 3-D empirical radiation pattern using the inverse DFT for the pyramidal horn antenna .....                                | 17 |
| Fig. 18 | Mean RMSE of the reconstructed 3-D radiation pattern using the inverse DFT for the pyramidal horn antenna (anechoic chamber) .....      | 18 |

## 1. Introduction

---

Far-field radiation patterns are an essential part of antenna characterization. Usually, the process of measuring 2-dimensional (2-D) or 3-dimensional (3-D) radiation patterns is time consuming and expensive. For instance, a complete 3-D radiation pattern with a spatial resolution in  $\theta$  and  $\phi$  of  $2^\circ$  requires 16,200 measurements. Measuring a complete 3-D radiation pattern with a resolution of  $2^\circ$  in both directions in an anechoic chamber can take up to 5 hours (h). The need for a process or algorithm that will reduce the number of samples required to reconstruct a far-field radiation pattern is thus identified.

In the literature, several techniques to approximate radiation patterns can be found. Classical interpolation methods have been explored—such as the one used by Werner.<sup>1</sup> He proposed a method to interpolate 3-D radiation patterns using a Model-Based Parameter Estimation (MBPE) technique that reduces the computational time required to model radiation patterns. Another method was proposed by Mikas,<sup>2</sup> where he compared different mathematical interpolation methods to reconstruct 3-D radiation patterns from the 2 principal cuts; however, an error analysis with respect to the true radiation pattern was not performed to evaluate the proposed interpolation method.

Other approaches exist including interpolation and extrapolation methods that reduce the amount of time required to model radiation patterns by using computer software simulations.<sup>3</sup> However, limited approaches have been investigated on the reduction of the number of experimental measurements for 2-D or 3-D radiation pattern reconstruction. For instance, Vasiliadis<sup>4</sup> introduced a new technique for approximating 3-D radiation patterns by combining the 2 principal cuts. This method uses extrapolation to approximate 3-D radiation patterns. Lawrence<sup>5</sup> proposed a method that uses compressive sensing to reconstruct the antenna radiation pattern. However, the proposed method makes use of 2 parallel plates to perform the measurements and the measurements were performed by using random sensors, which makes the method difficult for real data measurements.

In this report, an algorithm based on compressive sensing is proposed to perform the sensing and the compression of far-field radiation patterns. The reconstruction algorithm uses the inverse Discrete Fourier Transform (DFT) or inverse Discrete Cosine Transform (DCT) to recover the far-field radiation pattern. By using the proposed algorithm a complete reconstruction of either the 2-D or 3-D far-field radiation pattern is obtained—reducing the number of measurements and the time required to reconstruct a far-field radiation pattern.

## 2. Compressive Sensing Theory

---

Compressive sensing has been widely used to overcome sampling restrictions for a wide variety of applications.<sup>6-8</sup> Compressive sensing is a method that is used to sample a signal-of-interest at rates that can be lower than that required by the Nyquist criterion and still able to reconstruct the complete signal.<sup>9</sup>

Consider a signal  $\mathbf{x}$  of size  $N \times 1$  that can be represented in terms of a basis matrix  $\Psi$  of size  $N \times N$ . Then  $\mathbf{x} = \Psi \mathbf{s}$ , where  $\mathbf{s}$  is a vector of size  $N \times 1$ . The signal  $\mathbf{x}$  is said to be sparse if  $K < N$  coefficients of the vector  $\mathbf{s}$  are nonzero. In such case, the signal  $\mathbf{x}$  can be compressed by using compressive sensing.

The number of measurements required to reconstruct the signal  $\mathbf{x}$  can be reduced by taking  $\mathbf{y} = \mathbf{Ax} = \mathbf{A}\Psi \mathbf{s} = \Theta \mathbf{s}$  measurements, where  $\mathbf{y}$  is a vector of size  $M \times 1$ ,  $M$  is the number of measurements less than  $N$ ,  $\mathbf{A}$  is the matrix used to keep the basic functions associated with the measurements, and  $\Theta = \mathbf{A}\Psi$ . The approximation of the  $\mathbf{x}$  signal in the sparse domain,  $\hat{\mathbf{s}}$  is accomplished by solving the  $\ell_1$ -minimization problem  $\hat{\mathbf{s}} = \min \|\mathbf{s}\|_1$  such that  $\Theta = \hat{\mathbf{s}} \mathbf{y}$ , with the  $\ell_p$ -norm of a vector  $\mathbf{f}$  defined as  $\|\mathbf{f}\|_p = (\sum_{j=1}^N |f_j|^p)^{1/p}$ , where  $p \geq 1$ . In the case that  $p = 0$ , the  $\ell_0$ -norm is the number of nonzero elements in  $\mathbf{s}$ .

### Compressive Sensing Applied to Far-Field Radiation Patterns

---

A signal is said to be compressible if we can find a basis representation of the measured signal—in this case the radiation pattern—that is sparse. A far-field radiation pattern is a representation of the intensity of the field with respect to  $\theta$  and  $\phi$  given by  $f(\theta, \phi)$ . Consider a 2-D radiation pattern  $f(\theta)$  with a fixed  $\phi$ . In this case, the radiation pattern represents a cut of the 3-D radiation pattern. A basis representation of  $f(\theta)$  in another domain where it is sparse is required to apply the reconstruction compressive sensing algorithm. In addition, designing the measurement matrix is a key factor in the radiation pattern recovery using compressive sensing. The measurement matrix used should follow the restricted isometry property (RIP) to ensure recovery.<sup>9</sup> One measurement matrix that has been used in compressive sensing applications that follow the RIP is the random partial Fourier matrix.<sup>10-12</sup> The random partial Fourier matrix is derived from the DFT given by

$$f(n) = \sum_{k=0}^{N-1} F(k) e^{-j2\pi kn/N}, \quad (1)$$

where  $n$  is the index of the radiation pattern angle,  $k$  is the index of the transform domain, and  $N$  is the total number of samples.

In the case of a measured far-field radiation pattern,  $f(\theta)$  is a vector of size  $N \times 1$ ; therefore, the inverse DFT can be represented as an operator in matrix form such that  $\mathbf{x} = \mathbf{T}\mathbf{s}$ , where  $\mathbf{s}$  is the transform domain that contains  $K < N$  nonzero values and  $\mathbf{T} = \mathbf{T}_{\text{DFT}}$  or  $\mathbf{T}_{\text{DCT}}$  is the matrix representation of the inverse DFT given by

$$T_{DFT} = \frac{1}{\sqrt{N}} \begin{bmatrix} e^{i2\pi n_0 k_0/N} & \dots & e^{i2\pi n_0 k_{N-1}/N} \\ \vdots & \ddots & \vdots \\ e^{i2\pi n_{N-1} k_0/N} & \dots & e^{i2\pi n_{N-1} k_{N-1}/N} \end{bmatrix}. \quad (2)$$

Another transform that can be used as a basis function in compressive sensing is the DCT. The inverse DCT transform follows the RIP property, which guarantees recovery of the signal by using compressive sensing with enough uniformly random measurements.<sup>9</sup> The inverse DCT can be performed by using a matrix  $\mathbf{T}_{\text{DCT}}$  defined as

$$T_{DCT} = \frac{1}{\sqrt{N}} \begin{bmatrix} 1 & \dots & 1 \\ \cos \left[ \frac{(2k_0+1)n_1\pi}{2N} \right] & \ddots & \cos \left[ \frac{(2k_{N-1}+1)n_1\pi}{2N} \right] \\ \cos \left[ \frac{(2k_0+1)n_{N-1}\pi}{2N} \right] & \dots & \cos \left[ \frac{(2k_{N-1}+1)n_{N-1}\pi}{2N} \right] \end{bmatrix}. \quad (3)$$

The inverse DFT or inverse DCT matrix can be converted to a partial random matrix by randomly selecting the rows of the inverse DFT matrix or inverse DCT matrix.<sup>12,13</sup> The random rows are created by using a uniform random distribution. The measurement of the radiation pattern is performed by using  $M$  number of measurements where  $M < N$ , given as a result of matrix  $M \times N$ . As can be seen, the sensing of the radiation pattern is already incorporated into the compressive sensing algorithm, where only  $M$  samples are randomly measured. Ultimately, the measured samples are used as the input to the compressive sensing algorithm to reconstruct the radiation pattern with a minimal reconstruction error.

For the case of 3-D radiation patterns, the goal is to reduce the number of samples in both the  $\theta$  and  $\phi$  directions. Assume that the matrix containing the 3-D radiation pattern information is  $N \times L$ . A traditional 2-D compressive sensing algorithm converts the matrix into a long 1-dimensional (1-D) vector to perform the reconstruction. Although this may work for other applications, vectorizing the matrix will reduce the number of measurements only in 1 direction and add complexity to the reconstruction in the radiation pattern.<sup>9</sup> A method where parallel compressive sensing is used to overcome vectorization limitations was proposed by Fang, where the reconstruction is performed by using compressive sensing column by column.<sup>14</sup> However, by using this method, the reduction of the number of measurements is performed only in 1 direction. Therefore, a 2-step process is proposed, where random measurements are taken in both directions resulting in a

matrix  $M \times P$ , where  $M < N$  and  $L < P$ , obtaining a reduction in both directions  $\theta$  and  $\phi$ . The 3-D radiation pattern reconstruction is performed first in the  $\phi$  direction for each measured  $\theta$ , where each 2-D cut is reconstructed using parallel compressive sensing for each row. Then, the 2-D cuts are reconstructed by using the columns of the matrix, resulting in a 3-D radiation pattern with size  $N \times L$  (Fig. 1).

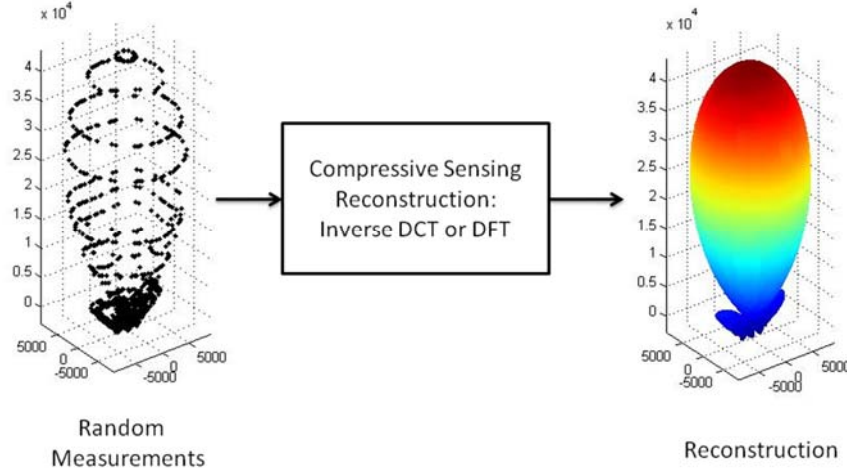


**Fig. 1 Compressive sensing algorithm for 3-D radiation patterns**

To evaluate the performance of the compressive sensing algorithm the root mean square error (RMSE) was used as

$$RMSE = \sqrt{\frac{1}{N} \sum_{n=1}^N \mathbf{f}_n - \hat{\mathbf{f}}_n}, \quad (4)$$

where  $\mathbf{f}_n$  is the simulated radiation pattern in HFSS and  $\hat{\mathbf{f}}_n$  is the reconstructed radiation pattern.

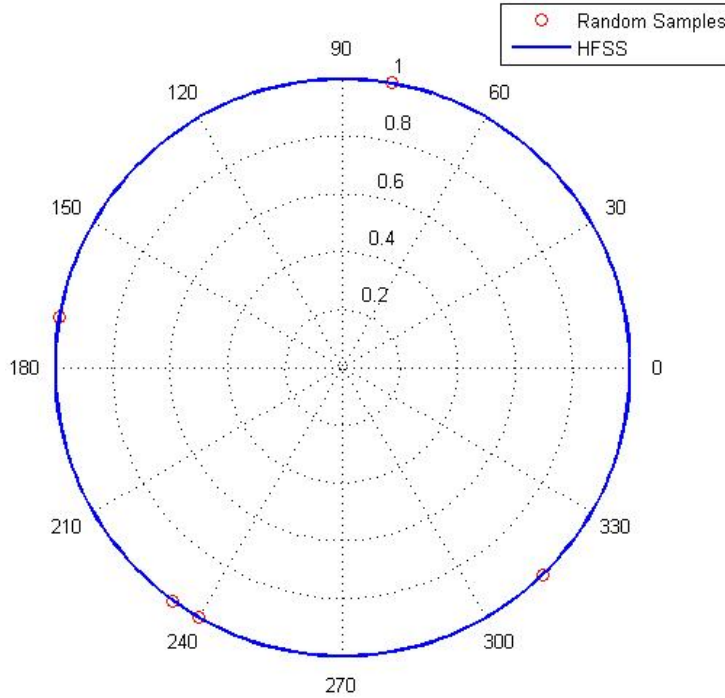
### 3. Evaluation of the Compressive Sensing Reconstruction Algorithm by Simulation

The compressive sensing algorithm was evaluated using 3 antennas: the half-wave dipole, the Vivaldi, and the pyramidal horn. The  $E_{\text{total}}$  far-field radiation patterns of the antennas were simulated in HFSS and exported to Matlab. The compressive sensing algorithm was applied for each radiation pattern. The half-wave dipole and the horn antennas were designed at a center frequency of 1.35 GHz, the Vivaldi antenna was designed at a center frequency of 6 GHz. The radiation pattern for each antenna was simulated at a resolution of  $2^\circ$  in both the  $\theta$

and  $\phi$  directions; therefore,  $181 \times 91$  is considered the total number of samples to be reconstructed.

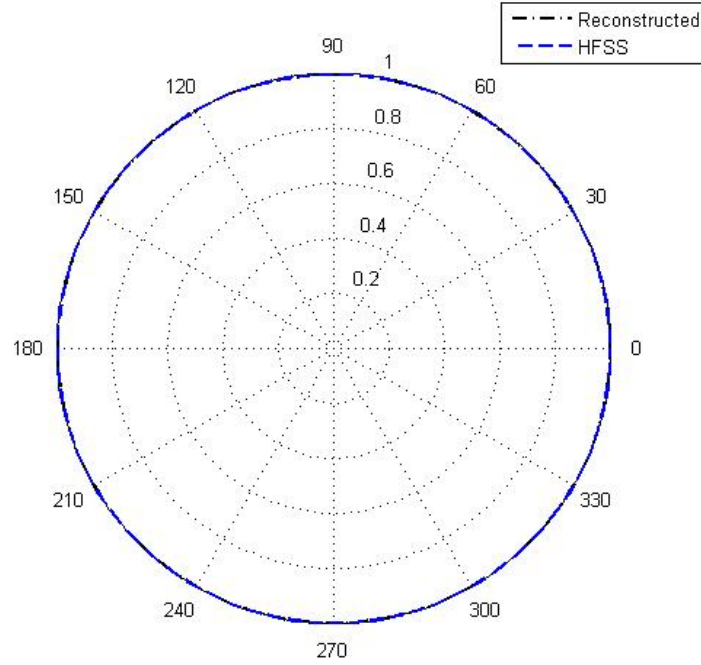
### 3.1 Half-Wave Dipole Antenna

The 2-D radiation pattern of a half-wave dipole antenna was reconstructed by using compressive sensing. The compressive sensing approach was used to reconstruct the 2 principal cuts of the radiation pattern. Figure 2 shows the simulated radiation pattern for  $\theta = 90^\circ$  and the  $x$  random measurements used for reconstruction.



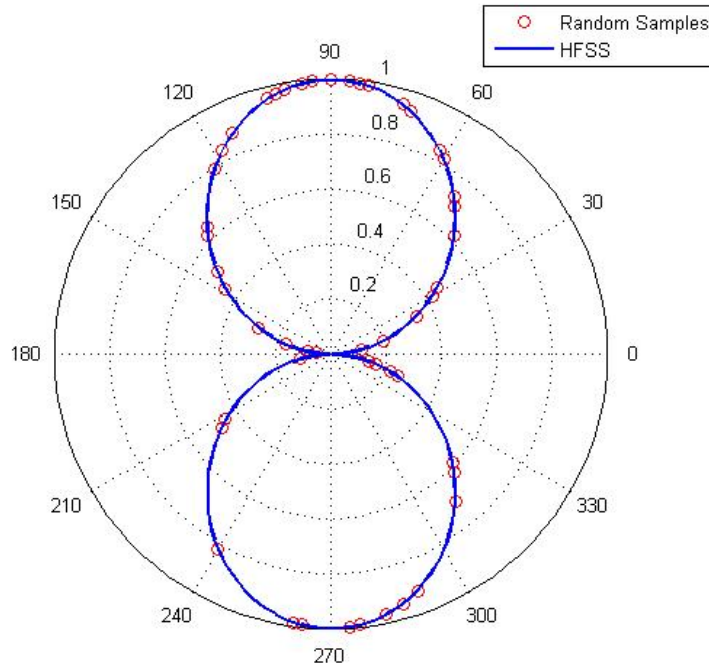
**Fig. 2** Random samples taken from the simulated 2-D radiation pattern of a vertical half-wave dipole at  $\theta = 90^\circ$

Figure 3 shows the reconstructed and simulated radiation patterns. The inverse DFT matrix was used for the reconstruction. In this case, 5 random samples are required to reconstruct the 2-D radiation pattern, which is less than 3% of the total number of samples. The RMSE of the reconstructed radiation pattern is  $1.6 \times 10^{-5}$ . The symmetry property and simplicity of the 2-D radiation pattern of the half-wave dipole make the compressive sensing reconstruction easier and faster.



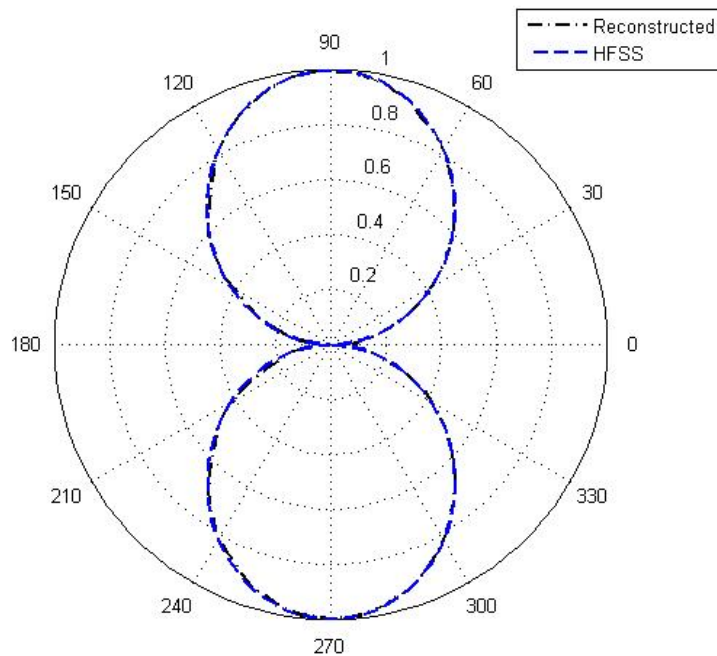
**Fig. 3** Reconstructed radiation pattern compared to the simulated radiation pattern of a vertical half-wave dipole at  $\theta = 90^\circ$

Figure 4 shows the simulated 2-D radiation pattern for  $\phi = 0$  and the samples used for reconstruction.



**Fig. 4** Random measurements taken from the simulated radiation pattern of a horizontal half-wave dipole at  $\phi = 0^\circ$

The reconstructed radiation pattern using the inverse DFT matrix for the compressive sensing reconstruction algorithm is shown in Fig. 5. In this case 50 samples were used to reconstruct the radiation pattern by using the compressive sensing algorithm—that is, 27% of the total number of samples with an RMSE of  $4.3 \times 10^{-5}$ .



**Fig. 5** Reconstructed radiation pattern compared to the simulated radiation pattern of a horizontal half-wave dipole at  $\phi = 0^\circ$

There is a tradeoff between the number of measurements required to obtain a reconstruction of the radiation pattern and the RMSE of that pattern. The sensing of the radiation pattern performs random measurements of the radiation pattern. To explore this relationship, a Montecarlo simulation was designed where the mean of the RMSE of reconstruction was calculated as the number of measurements  $M$  was increased. The experiment was repeated 1,000 times for each number of measurements and the RMSE averaged. Figure 6 shows the mean RMSE with respect to the normalized number of measurements when the inverse DFT and the inverse DCT were used. We can observe that the mean RMSE converges to zero faster when using the inverse DFT than by using the inverse DCT.

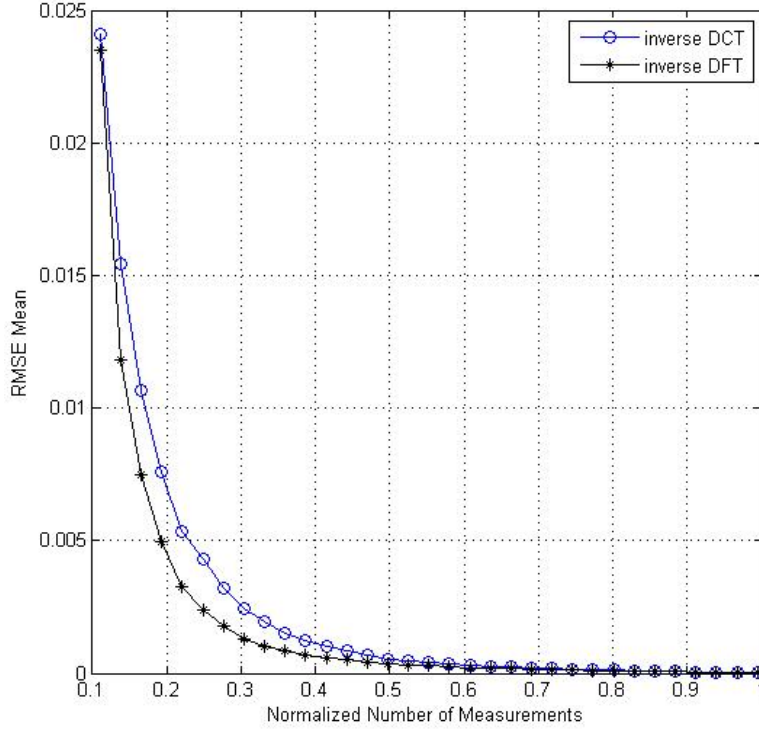


**Fig. 6** Mean RMSE of the reconstructed radiation pattern for the horizontal half-wave dipole for  $\phi = 0^\circ$

### 3.2 Vivaldi Antenna

The half-wave dipole has a simple radiation pattern that can be perfectly reconstructed by using the proposed compressive sensing algorithm. A more complicated radiation pattern was obtained by modeling the Vivaldi antenna. One of the principal cuts of the 2-D radiation pattern of the Vivaldi antenna was simulated in HFSS. The radiation pattern and the samples used for the compressive sensing reconstruction are shown in Fig. 7.

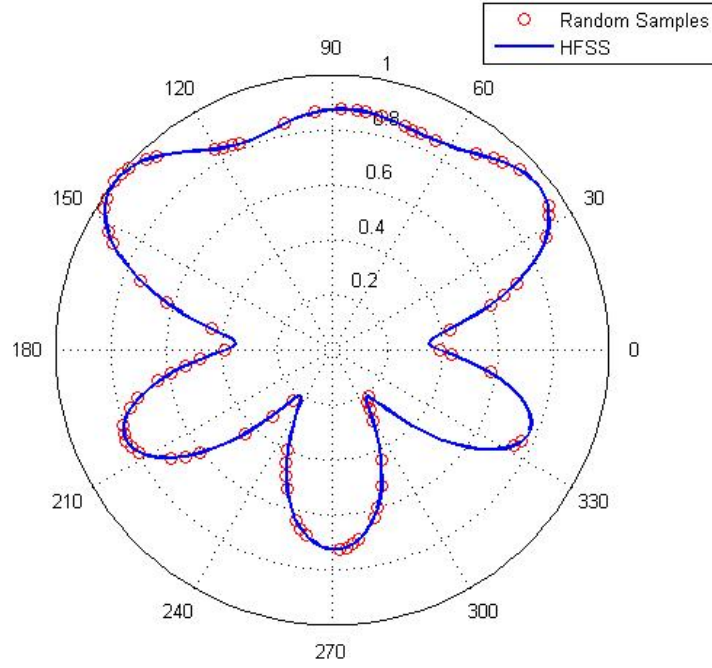


**Fig. 7 Simulated radiation pattern and random samples used for reconstruction of the Vivaldi antenna**

The reconstructed radiation pattern is shown in Fig. 8. In this case the inverse DFT and 70 samples were used for reconstruction—that is, 38% of the total samples are required to obtain a reconstruction with an RMSE of  $9.87 \times 10^{-6}$ .

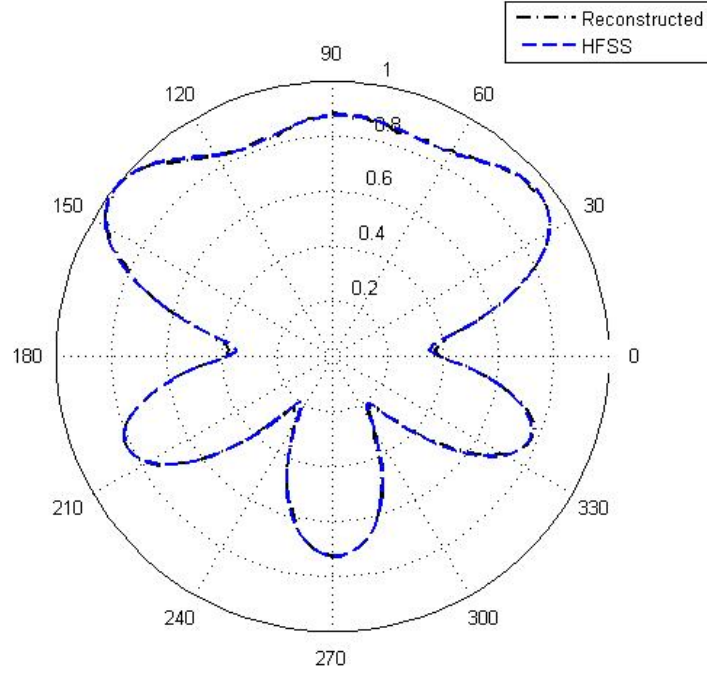


**Fig. 8 Simulated radiation pattern and reconstructed radiation pattern of the Vivaldi antenna**

The mean RMSE was calculated for a Montecarlo simulation of 1,000 realizations as the number of measurements was increasing. Figure 9 shows the comparison of the inverse DFT and the inverse DCT compressive sensing algorithms. As noted, the reconstruction obtained when using the inverse DFT converges to zero more quickly. However, more samples are required to obtain a good reconstruction compared to the half-wave dipole antenna.

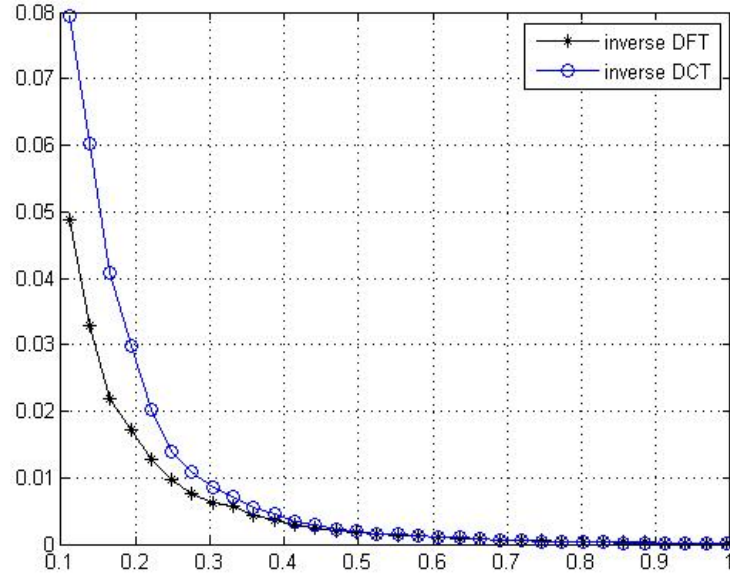


**Fig. 9** RMSE mean of the reconstructed radiation pattern for the Vivaldi antenna

### 3.3 Pyramidal Horn Antenna

A pyramidal horn antenna pattern was used to test the compressive sensing algorithm. The simulated radiation pattern and the random measurements taken are shown in Fig. 10. In this case 80 samples were used as the number of measurements, 44% for the total data points. This yielded an RMSE of  $4.74 \times 10^{-6}$ .

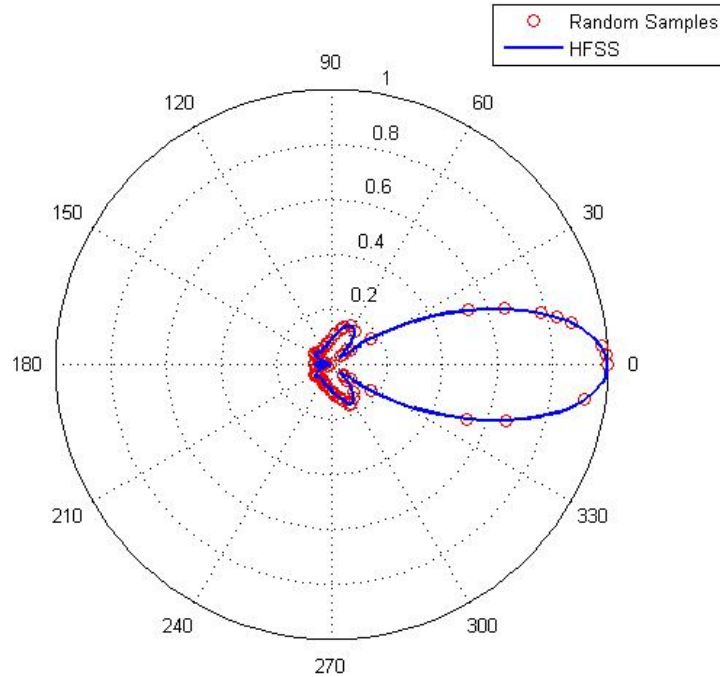


**Fig. 10** Simulated radiation pattern and measurements taken for the horn antenna

Figure 11 shows the simulated radiation pattern compared to the reconstructed radiation pattern. A close approximation of the radiation pattern was obtained for the horn antenna.

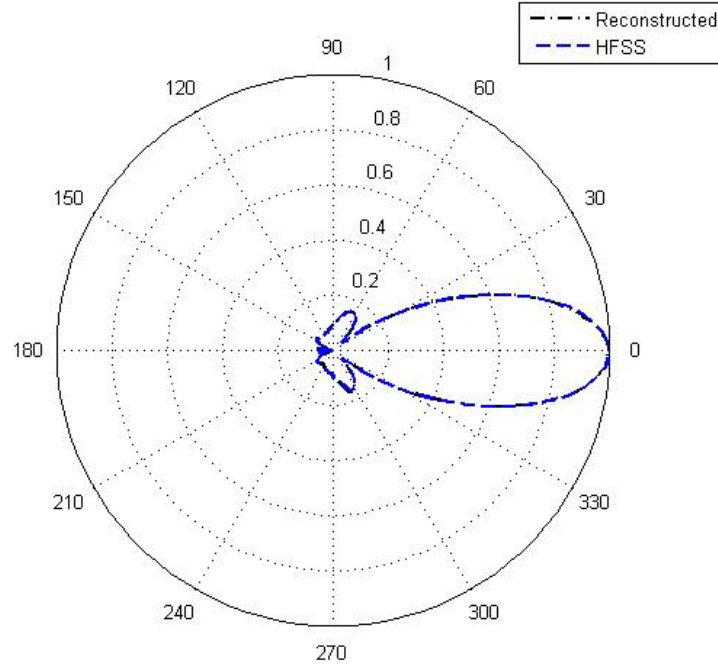


**Fig. 11 Simulated radiation pattern and reconstructed radiation pattern for the horn antenna**

The RMSE mean was calculated as the number of measurements was increased. A Montecarlo simulation of 1,000 trials was used to obtain the mean RMSE of the reconstructed radiation pattern with the inverse DFT and inverse DCT. The results are shown in Fig. 12. The 2 reconstruction basis matrices give similar results as the 2 converge to zero in approximately the same manner.

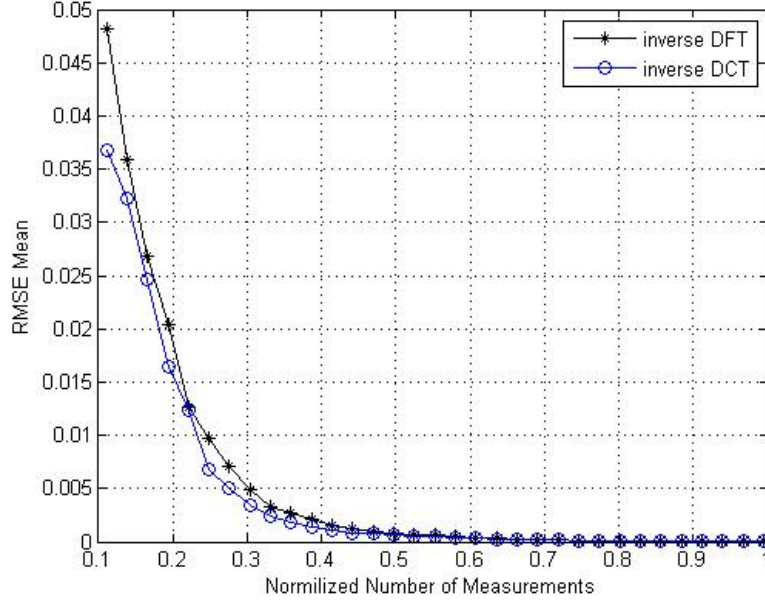
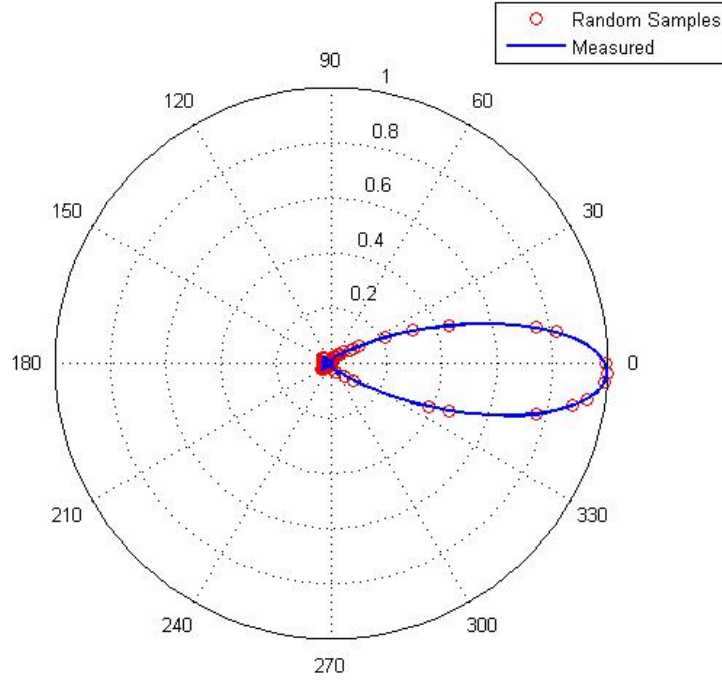


Fig. 12 RMSE mean of the reconstructed radiation pattern for the horn antenna

#### 4. Evaluation of the Compressive Sensing Reconstruction Algorithm by Experiment

A pyramidal horn antenna (having the same dimensions as the horn antenna simulated in HFSS) was used to test the compressive sensing algorithm experimentally. The antenna frequency range is 1.12–1.70 GHz, and the transmitted frequency used was 1.35 GHz. To test the compressive sensing reconstruction algorithm, the radiation pattern was measured at a resolution of  $2^\circ$  in both the  $\theta$  and  $\phi$  directions. The radiation pattern of the antenna was measured in the anechoic chamber. The 2-D and 3-D radiation pattern measurements were used to test the compressive sensing algorithm in an empirical scenario. The measured 2-D radiation pattern and the random samples used for reconstruction are shown in Fig. 13. Note the lack of back-lobe measurement due to the presence of the supporting tower.



**Fig. 13 2-D radiation pattern of the pyramidal horn (anechoic chamber) antenna and measurements used for reconstruction**

To reconstruct the 2-D radiation pattern, 80 samples—that is, 46% of the total samples—with an RMSE of  $9.28 \times 10^{-4}$  were used (the same number of samples as used in the simulated radiation pattern of the horn antenna). The 2-D radiation pattern reconstruction and the measured radiation pattern are shown in Fig. 14.

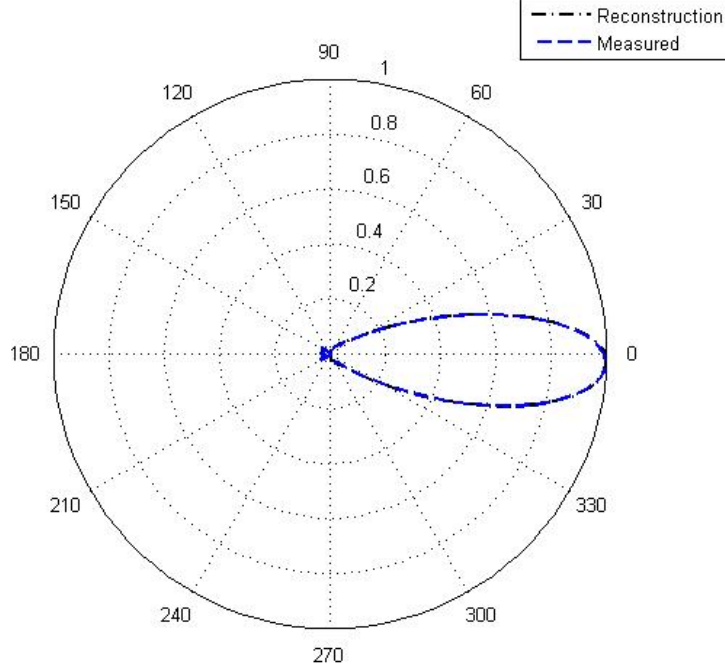


**Fig. 14** Anechoic chamber radiation pattern and reconstructed radiation pattern for the pyramidal horn antenna

The mean RMSE was calculated for the 2-D reconstruction of the pyramidal horn antenna. The error between the reconstructed radiation pattern using compressive sensing ( $K$  = random measurements) and the measured radiation pattern ( $N$  = number of measurements) is shown in Fig. 15. The mean RMSE was obtained from a Montecarlo simulation of 1,000 realizations of the experiment. The compressive sensing reconstruction algorithm performs a similar reconstruction for both the inverse DFT matrix and the inverse DCT because both tend to converge to zero at about the same time.

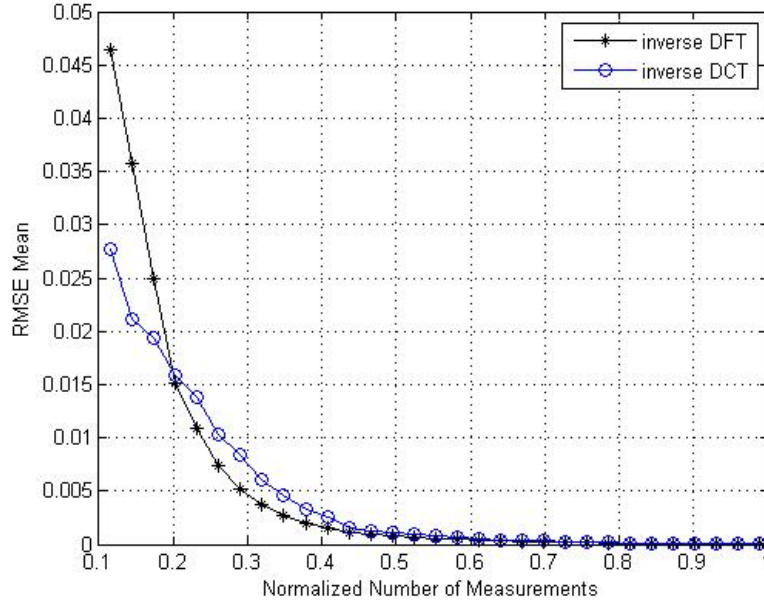


**Fig. 15** Mean RMSE of the reconstructed empirical radiation pattern for the pyramidal horn antenna

Figure 16 shows the measured radiation pattern (anechoic chamber) and the random samples used for reconstruction by using compressive sensing.

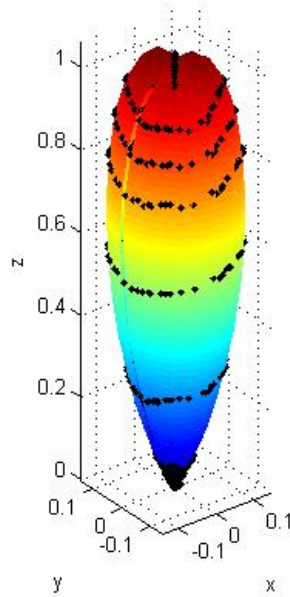


**Fig. 16** The empirical 3-D radiation pattern and samples used for reconstruction for the pyramidal horn antenna

The random samples were used to reconstruct the 3-D radiation pattern of the horn antenna. The 2-step process was used where 30 measurements were taken along  $\theta$  and 70 measurements were taken along  $\phi$ . Because the inverse DFT and the inverse

DCT provide similar results when reconstructing the radiation pattern of the horn antenna, only the inverse DFT was used for the 3-D reconstruction.

A total of 2,100 samples were taken from a total of 16,200 samples considering resolution of  $2^\circ$  in both directions. The reconstructed 3-D radiation pattern is shown in Fig. 17. The reconstructed 3-D radiation pattern resembles the original radiation pattern.

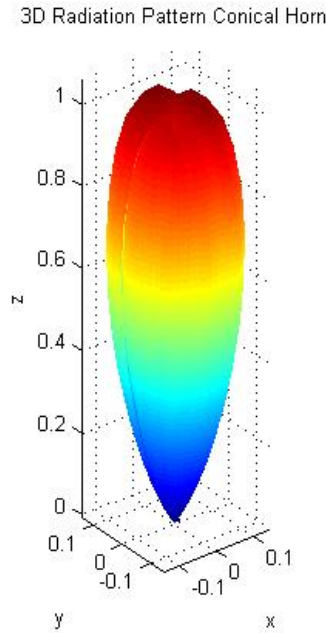


**Fig. 17 Reconstructed 3-D empirical radiation pattern using the inverse DFT for the pyramidal horn antenna**

The 3-D radiation pattern reconstruction was evaluated by using the RMSE. A Montecarlo simulation was performed where the number of measurements along the  $\theta$  was fixed to 30 as the number of measurements along  $\phi$  was increased. The RMSE mean was calculated for each 2-D radiation pattern cut  $f(\phi)$  of the 3-D pattern. The process was repeated 100 times to obtain the mean RMSE for each  $\phi$  as the number of measurements increased. Figure 18 shows the results. As observed, the mean RMSE approaches zero after 0.4 normalized number of measurements. The mean RMSE is higher at the region where  $\phi$  is close to zero.

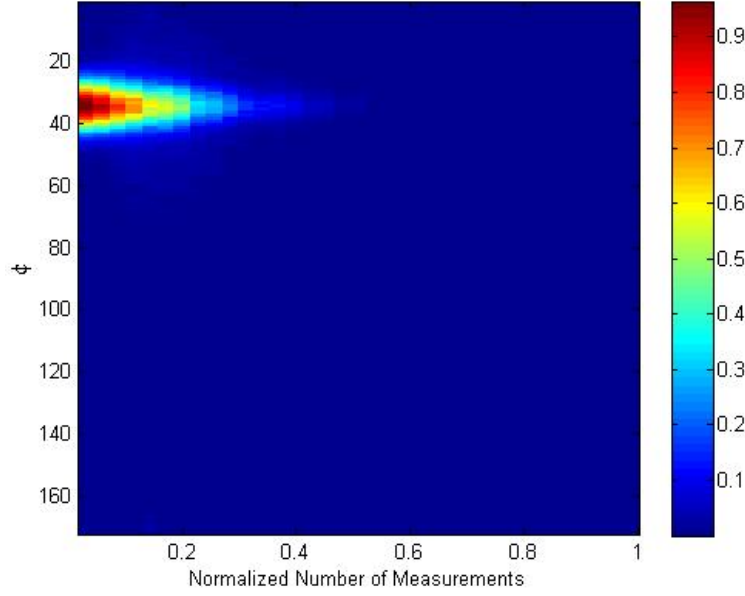


**Fig. 18** Mean RMSE of the reconstructed 3-D radiation pattern using the inverse DFT for the pyramidal horn antenna (anechoic chamber)

## 5. Conclusions

A compressive sensing algorithm that performs the sensing and the compression of 2-D or 3-D radiation patterns was presented. The 2-D radiation pattern of a half-wave dipole can be recovered by using only 3% of the total number of samples. Directive antennas such as the Vivaldi and the horn antennas have more complex radiation patterns compared to the half-wave dipole. Therefore, the 2-D radiation patterns will need more measurements, and can be reconstructed by using less than 44% of the total number of samples. The compression rate, or the number of random measurements required for a good reconstruction, depends on the radiation pattern structure. Two basis matrices—the inverse DFT and the inverse DCT—were evaluated for the reconstruction of radiation patterns. From simulations, it can be concluded that both matrices perform similar reconstructions of the radiation patterns.

The algorithm was evaluated empirically by measuring a pyramidal horn antenna, where 2-D and 3-D radiation patterns measured in the anechoic chamber were reconstructed by using the proposed reconstruction algorithm. The 2-D radiation pattern was reconstructed by using 44% of the total data, and the 3-D radiation pattern was reconstructed by using 13% of the total number of samples. The measurement of a 3-D radiation pattern takes more than 5 h in an anechoic chamber. By using the compressive sensing algorithm the 3-D radiation pattern can be reconstructed with measurements taking less than 0.65 h. The proposed

reconstruction algorithm can be used to reconstruct 2-D or 3-D radiation patterns; therefore, reducing the number of required measurements to reconstruct the radiation pattern and reducing the time required to take the measurements.

A novel method to reconstruct measurements in an anechoic chamber was presented. The algorithm was tested with a measured 3-D radiation pattern. The implementation of the algorithm requires the implementation of a new measurement paradigm that will perform random measurements in the anechoic chamber. By using the proposed methodology, the time required to measure radiation patterns can be reduced by 1/5 of the total time without significant loss of accuracy.

## 6. References

---

1. Werner DH, Allared RJ. The simultaneous interpolation of antenna radiation patterns in both the spatial and frequency domains using model-based parameter estimation. *IEEE Antennas and Propagation*. 2000;48(3):196.
2. Mikas F, Pechac P. The 3-D approximation of antenna radiation patterns. *IEEE Transactions on Signal Processing*. 2013;62:196.
3. Herscovici N, Christodouiou C. A 3-D interpolation method for base-station antenna radiation patterns. *IEEE Antennas Propagation Magazine*. 2001;43(2):132.
4. Vasiliadis TG, Dimitriou D, Sergiadis JD. A novel technique for the approximation of 3-D antenna radiation patterns. *IEEE Transactions on Antennas and Propagation*. 2005;53(7).
5. Carin L, Liu D, Gua B. In situ compressive sensing. *IEEE Science Inverse Problems*. 2008;24.
6. Romberg J. Imaging via compressive sampling. *IEEE Antennas Propagation Magazine*. 2008;25(2):14.
7. Trzasko J, Manduca A, Borisch E. Highly under-sampled magnetic resonance image reconstruction via homotopic ell-0-minimization. *IEEE Transactions Medical Imaging*. 2009;28(1):106.
8. Baraniuk R, Steeghs P. Compressive radar imaging. 2007.
9. Baraniuk R. Compressive sensing. *IEEE Signal Processing Magazine*. 2007;24:118.
10. Candes EJ, Tao T, Romberg J. Robust uncertainty principles: Exact signal reconstruction from highly incomplete frequency information. *IEEE Transactions on Inform. Theory*. 2006;52(2):489.
11. Candes EJ, Tao T. Near optimal signal recovery from random projections: Universal encoding strategies. *IEEE Transactions on Inform. Theory*. 2006;52(12):5406.
12. Fornasier M, Rauhut H. Compressive sensing. *Handbook of Mathematical Methods in Imaging*. 2010:187, 2010.
13. Rauhut H. Compressive sensing and structural random matrices. *Theoretical Foundations and Numerical Methods for sparse recovery*. p. 1, 2010.

14. Fang H, Vorobyov SS, Jiang H, Taheri O. Permutation meets parallel compressed sensing: How to relax restricted isometry property for 2-D sparse signals. Proc. Inst. Elect. Eng. 12th Int. Conf. Antennas Propagation ICAP, p. 751, 2003.

## List of Symbols, Abbreviations, and Acronyms

---

|      |                                     |
|------|-------------------------------------|
| 1-D  | 1-Dimensional                       |
| 2-D  | 2-Dimensional                       |
| 3-D  | 3-Dimensional                       |
| DCT  | Discrete Cosine Transform           |
| DFT  | Discrete Fourier Transform          |
| h    | hour(s)                             |
| HFSS | high-frequency structural simulator |
| MBPE | Model-Based Parameter Estimation    |
| RIP  | restricted isometry property        |
| RMSE | root mean square error              |

|                                 |  |
|---------------------------------|--|
| 1<br>(PDF)                      | DEFENSE TECHNICAL<br>INFORMATION CTR<br>DTIC OCA                             |
| 2<br>(PDF)                      | DIRECTOR<br>US ARMY RSRCH LAB<br>RDRL CIO LL<br>IMAL HRA MAIL & RECORDS MGMT |
| 1<br>(PDF)                      | GOVT PRINTG OFC<br>A MALHOTRA  |
| 1<br>(PDF)<br>1 WORD<br>VERSION | US ARMY RSRCH LAB<br>MELE ASSOCIATES INC<br>ATTN RDRL SLE E<br>D NEVAREZ     |
| 2<br>(PDF)                      | RDRL SLE E<br>P DEBROUX<br>B VERDIN  |

INTENTIONALLY LEFT BLANK.